This article has been accepted for publication in IEEE Transactions on Antennas and Propagation. This is the author's version which has not been fully edited and content may change prior to final publication. Citation information: DOI 10.1109/TAP.2023.3333956

Simultaneous Maximization of Voltage and Power Efficiencies in Magneto-Mechanical Transmitters

Jiheng Jing *Graduate Student Member, IEEE,* and Gaurav Bahl, *Senior Member, IEEE*

***Abstract*—Magneto-mechanical resonator arrays have emerged as a promising transmitter solution for compact ultra-low frequency (ULF) wireless communication systems and can be extremely power-efficient compared to traditional electrical antennas in the ULF range. The efficiency of ULF signal generation using magneto-mechanical transmitters (MMTs) is dictated by multi-physical effects from mechanical, magnetic, and electrical domains, leading to an interesting trade space. In this work, we show that an MMT's most power-efficient and most voltage-efficient driving frequencies always differ, forcing designers to sacrifice one efficiency for the other. To address this issue, we propose an efficiency optimization method that minimizes the total impedance of the MMT at the most power-efficient driving frequency, by means of a compensation capacitor added to the electromagnetic actuation coil system. Our experimental results show excellent agreement with our analytical model, and we demonstrate that our approach enables simultaneous maximization of voltage and power efficiencies of an MMT at the same driving frequency. We additionally describe how to apply this optimization method on multi-resonator magneto-mechanical arrays and present numerical analysis that predicts much greater improvement factors in systems having larger net magnetic moments and drive coils with larger sizes.**

***Index Terms*—Ultra-low frequency (ULF) transmitters, wireless communication, magneto-mechanical systems.**

I. Introduction

WIRELESS data transfer plays a valuable role in our daily activities. However, wireless communications are particularly important for marine and underground activities, including search and rescue, locator beacons, and environmental monitoring. Unfortunately, radio signals cannot propagate through conductive media such as seawater, metal, rock, and soil due to significant signal attenuation [1]. In this context, ultra-low frequency (ULF, < 3 kHz) communication systems have been shown as a good alternative due to the very large skin depth at ULF, which significantly enhances the range. The difficulty arises with traditional electrical antennas since, when scaled for ULF, they require a very large area [2] and prohibitive power for generating sufficient signal levels [3], [4], making them impractical for many real-world applications. Recently, a fundamentally new approach to building ULF transmitters has been developed [5]–[12], commonly referred to as magneto-mechanical transmitters (MMT). In an MMT, the magnetic field carrier signal is generated through the angular motion of permanent magnetic dipoles, on which data can be encoded using amplitude or frequency modulations. Since the permanent magnetic dipole brings the power requirement for generating the magnetic field to exactly zero, the power dissipation now only appears in the driving mechanism [5], the mechanical losses in the suspension system [13], and the eddy current losses in the magnetic materials [14]. Notably, as the mechanical oscillation frequency decreases, the associated mechanical loss and eddy current loss also decrease rapidly. Therefore, MMTs provide a power-efficient alternative to traditional electrical antennas for ULF transmitters.

A typical oscillatory MMT consists of a drive coil and a magneto-mechanical resonator array (MMRA) [14] as shown in Fig. 1a. The MMRA can be designed with one or more rotors and stators, with the stators providing a restoring torque for resonant operation [5], [6]. An ac current provided to the coil produces an alternating magnetic field, generating an alternating torque on the rotors, which in turn leads to oscillatory motion. The resulting mechanical motion of the permanent dipoles produces a time-varying magnetic field at all points in space around the MMT, whose amplitude is directly related to the oscillatory amplitude of the rotors [5]. The driving frequency ω of the source is always set to be close to the mechanical resonant frequency of the MMRA [5], [6], [14] in order to achieve higher voltage efficiency, which can be expressed in terms of the time-varying magnetic field signal strength at the receiver normalized to the voltage level applied on the drive coil. We can also define power efficiency as the time-varying magnetic field signal strength normalized to the power dissipated in the MMT system. Both efficiency metrics are key for determining the practicality of MMTs, and both are functions of the driving frequency ω due to the resonance behavior of the MMRA as well as the coil [5]. In this paper, we observe that an MMT's most power-efficient and most voltage-efficient driving frequencies always differ, i.e. their resonances do not align, forcing designers to necessarily sacrifice one efficiency for the other. To address this issue, we propose an efficiency optimization method that minimizes the total impedance of the MMT at the most power-efficient driving frequency. Using experiments and analysis, we demonstrate that this method allows us to simultaneously maximize the voltage and power efficiencies of an MMT at the same driving frequency.

II. Power and Voltage Efficiencies of an MMT

We consider a single-rotor MMT as shown in Fig. 1a. The driving voltage, $V(t)$, is a sinusoid at frequency ω. The induced current in the coil, $I(t)$, and the resulting rotor motion, $\theta(t)$, can then generally be expressed as $I(t) = \frac{1}{2} I_m e^{j\omega t} + c.c.$

J. Jing and G. Bahl are affiliated with the Department of Mechanical Science and Engineering, University of Illinois at Urbana-Champaign, Urbana, IL 61801 USA (e-mail: bahl@illinois.edu).

This work is licensed under a Creative Commons Attribution 4.0 License. For more information, see https://creativecommons.org/licenses/by/4.0/

This article has been accepted for publication in IEEE Transactions on Antennas and Propagation. This is the author's version which has not been fully edited and content may change prior to final publication. Citation information: DOI 10.1109/TAP.2023.3333956

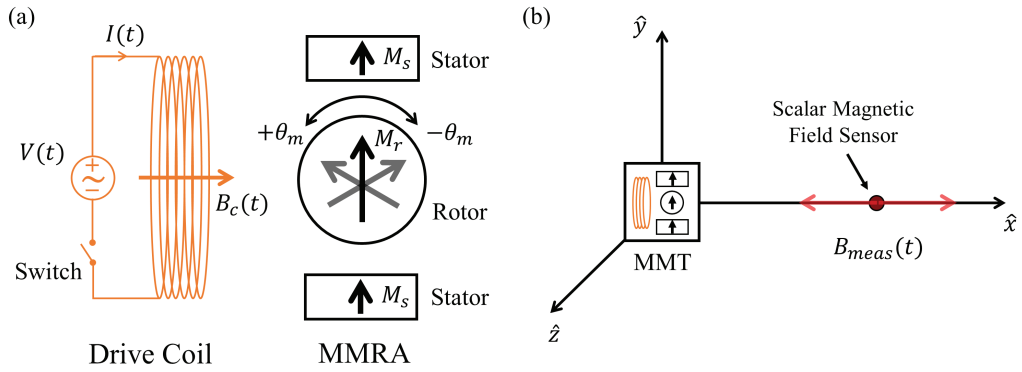

Fig. 1. The operational principle of an MMT. (a) Schematic diagram of a single-rotor MMT. The drive coil is supplied with an alternating voltage $V(t)$, which induces an alternating current $I(t)$ flowing through the coil. The drive coil generates an alternating magnetic field $B_c(t)$ in the $\hat{x}$ direction. The rotor and stators in the MMRA have uniform magnetization, M_r and M_s, respectively, pointing in the $\hat{y}$ direction at rest, which is orthogonal to $B_c(t)$ to maximize the driving torque on the rotor. During operation, stators remain static, and the rotor oscillates about its longitudinal axis with a time-varying angular position $\theta(t)$ with amplitude θ_m. The switch is used to implement the ON-OFF keying modulation. (b) Schematic diagram showing the relative position of the MMT and the receiver (scalar magnetic field sensor). The MMT generates a magnetic field at any point in space, $\vec{B}$, which varies with the angular position of the rotor magnet. The scalar magnetic field sensor is placed in the $\hat{x}$ direction to measure the projected magnetic field $B_{meas}(t)$ along the $\hat{x}$ direction.

and $\theta(t) = \frac{1}{2}\theta_m e^{j(\omega t+\phi)} + c.c.$ where I_m and θ_m are the current amplitude and the oscillation amplitude, respectively, and ϕ is some relative phase difference between $I(t)$ and $\theta(t)$. The configuration of MMT and receiver (x-oriented) shown in Fig. 1b has been previously discussed [5] as being the most optimal for generating the largest time-varying magnetic field at frequency ω. The x-oriented magnetic field measured at the receiver, $B_{meas}(t) = B_{MMRA}(t) + B_c(t)$, is comprised of the magnetic fields generated by both the MMRA and the coil. Under approximation that the angular motion of the MMRA dipole is relatively small, we can expand the sinusoidal using Taylor expansion and ignore the higher-order dependencies and simply write $B_{MMRA}(t) = A_\theta \theta(t)$ and $B_c(t) = A_I I(t)$ where A_θ and A_I are coefficients that describe the relationship between the magnetic fields and the current and rotor motion, whose values have been discussed in Ref. [14] and Ref. [15], respectively. The received magnetic signal can be defined as the RMS value of $B_{meas}(t)$:

$$B_{meas,\,rms} = \frac{1}{\sqrt{2}}|A_\theta \theta_m\, e^{j\phi} + A_I I_m|\ . \tag{1}$$

The average power consumed by the MMT can be evaluated as

$$P_{total,\,avg} = \frac{1}{2}R_c I_m^2 + \frac{1}{2}\beta\omega^2\theta_m^2 \tag{2}$$

where R_c is the resistance of the coil and β is the damping coefficient of the MMRA.

To quantify the power efficiency, we normalize the at-receiver magnetic signal strength to the average power consumed through the Field Per square Root Watt (FPRW) metric:

$$\text{FPRW}(\omega) = \frac{B_{meas,\,rms}}{\sqrt{P_{total,\,avg}}} = \frac{|A_\theta H_{\theta/I}(\omega) + A_I|}{\sqrt{R_c + \beta\omega^2|H_{\theta/I}(\omega)|^2}} \tag{3}$$

where $H_{\theta/I}(\omega)$ is the transfer function from the coil current to the angular position of the rotor. We take the square root of the average power in this expression since FPRW is independent of the input voltage level for a particular MMT. To quantify the voltage efficiency we similarly relate the at-receiver magnetic signal strength to the RMS value of the supplied voltage through the Field Per Volt (FPV) metric:

$$\text{FPV}(\omega) = \frac{B_{meas,\,rms}}{V_{rms}} = |H_{I/V}(\omega)| \cdot |A_\theta H_{\theta/I}(\omega) + A_I| \tag{4}$$

where $H_{I/V}(\omega)$ is the transfer function from the input voltage to the coil current. FPV(ω) also remains constant for an MMT regardless of the input voltage level. Since it is typical to use a voltage source to drive the coil [5], [6], the natural choice for driving frequency is where the FPV(ω) is maximized. We can find this resonance condition using Eq. 3, with the simplification that the damping coefficient β of the MMT is very small for most MMTs [5], [6], [14]. The denominator of FPRW(ω) is then dominated by the coil resistance R_c, implying that the shape of FPRW(ω) closely matches the shape of $H_{\theta/I}(\omega)$, which exhibits a resonance as we will see in the following paragraph. On the other hand, as can be seen in Eq. 4, the shape of FPV(ω) depends on both $H_{\theta/I}(\omega)$ and $H_{I/V}(\omega)$. Since $H_{\theta/I}(\omega)$ also exhibits a resonance, the most

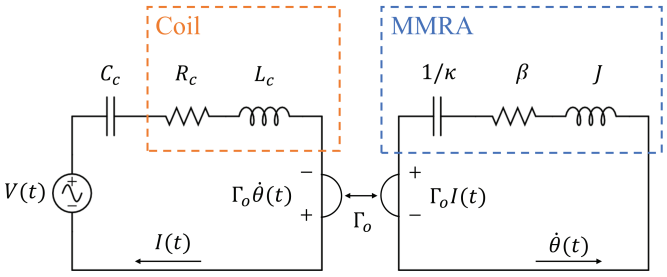

Fig. 2. Equivalent circuit model of the MMT. The circuit on the left models the driving system, and the circuit on the right models the MMRA. R_c and L_c are the resistance and inductance of the coil, respectively. C_c is the optional capacitance that can be introduced as a part of the driving system. κ, β, and J are the restoring stiffness, damping coefficient, and moment of inertia of the rotor, respectively. Two circuits are coupled through a gyrator [5], [16] where the coupling coefficient is Γ_o. The flow variables in the coil and MMT circuits are $I(t)$ and $\dot{\theta}(t)$, respectively. $V(t)$ in the coil circuit is the input voltage.

This work is licensed under a Creative Commons Attribution 4.0 License. For more information, see https://creativecommons.org/licenses/by/4.0/

This article has been accepted for publication in IEEE Transactions on Antennas and Propagation. This is the author's version which has not been fully edited and content may change prior to final publication. Citation information: DOI 10.1109/TAP.2023.3333956

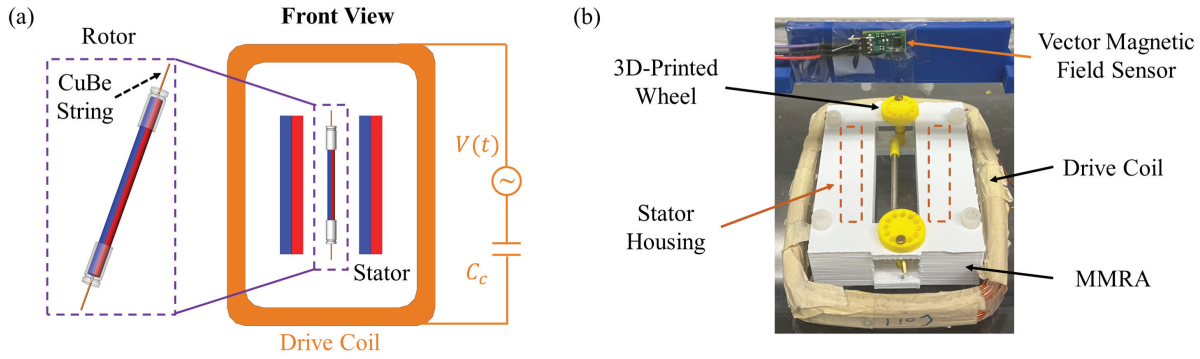

Fig. 3. (a) Schematic diagram of the single-rotor MMT. The single-rotor MMT uses a cylindrical neodymium magnet (NdFeB) as the rotor, two cuboidal NdFeB with a square cross-section as stators, and two copper beryllium (CuBe) wires as the suspension system. The drive coil is a 100-turn coil made of AWG 18 enameled copper wire and the capacitors are non-polarized ceramic capacitors. (b) Photograph of the experimental setup. The single-rotor MMT consists of a 3D-printed frame and two 3D-printed wheels to adjust the tension on the CuBe wires. We use a flux-gate magnetometer (Texas Instruments DRV425EVM) as the scalar magnetic field sensor to pick up the magnetic field signal as illustrated in Fig. 1b.

power-efficient and most voltage-efficient driving frequencies always differ, forcing the users to necessarily sacrifice one efficiency for the other. One approach to improve the FPV is by adding a step-up voltage transformer. However, adding a step-up transformer will not change the most power-efficient and most voltage-efficient driving frequencies and does not provide a solution to the problem.

To maximize FPRW(ω) and FPV(ω) at the same driving frequency, we need to match the resonant frequencies of $H_{\theta/I}(\omega)$ and $H_{I/V}(\omega)$. To accomplish this, we start from an equivalent circuit model [5] that describes the dynamical behavior of the system, as shown in Fig. 2. The circuit equations (all variables are defined in Fig. 2) can be written as

$$L_c\dot{I} + R_cI + \frac{1}{C_c}\int I dt = \Gamma_o\dot{\theta} + V \tag{5a}$$

$$J\ddot{\theta} + \beta\dot{\theta} + \kappa\theta = -\Gamma_o I\ . \tag{5b}$$

Here we have introduced an extra compensation capacitor C_c in series with the coil which we will use later to optimize the efficiencies with respect to drive voltage and power consumption. By converting to frequency domain, the transfer functions $H_{I/V}(\omega)$ and $H_{\theta/I}(\omega)$ can be evaluated as

$$H_{I/V}(\omega)^{-1} = \left[R_c + \frac{\Gamma_o^2\omega^2\beta}{\left(\kappa - J\omega^2\right)^2 + \left(\beta\omega\right)^2}\right] + j\left[\omega L_c - \frac{1}{\omega C_c} + \frac{\Gamma_o^2\omega\left(\kappa - J\omega^2\right)}{\left(\kappa - J\omega^2\right)^2 + \left(\beta\omega\right)^2}\right] \tag{6}$$

and

$$H_{\theta/I}(\omega) = \frac{\Gamma_o}{-J\omega^2 + j\omega\beta + \kappa}\ . \tag{7}$$

The resonance of $H_{\theta/I}(\omega)$ can be evaluated readily from Eq. 7 as $\omega_{res} = \sqrt{\frac{\kappa}{J} - \frac{\beta^2}{4J^2}} \approx \sqrt{\frac{\kappa}{J}}$ and is the same as the mechanical resonance frequency. We can similarly extract the spectral characteristics of the impedance function $H_{I/V}(\omega)$ by examining Eq. 6. With the assumption of small β, we can see that the Re$\{H_{I/V}(\omega)^{-1}\}$ will reach a minimum value R_c at the frequency at which Im$\{H_{I/V}(\omega)^{-1}\} = 0$. At this frequency, which we define as ω_{opt}, the function $H_{I/V}(\omega)$ will hit a resonance condition. Our optimization goal is now to find a compensation capacitor such that the resonance of $H_{I/V}(\omega)$ and of $H_{\theta/I}(\omega)$ are aligned, i.e. when $\omega_{opt} = \omega_{res}$. The value of this series capacitor C_c can then be found by setting Im$\{H_{I/V}(\omega_{res})^{-1}\} = 0$, resulting in the solution:

$$C_c = \left[\omega_{res}^2 L_c + \frac{\Gamma_o^2\omega_{res}^2\left(\kappa - J\omega_{res}^2\right)}{\left(\kappa - J\omega_{res}^2\right)^2 + \left(\beta\omega_{res}\right)^2}\right]^{-1}\ . \tag{8}$$

The slight deviation should appear due to the small β approximation that we applied earlier, which is best adjusted via experiments. As we will show later, this is not the same capacitance where the coil resonant frequency matches with the MMRA resonant frequency. It is also worth noting that irrespective of the compensation capacitor, the FPRW of the system is unaffected.

III. Experimental Results and Discussion

We have experimentally verified this optimization method using a single-rotor MMT. The MMT device is shown in Fig. 3, and values of experimental parameters used for efficiency calculations are measured and listed in Table I (other material properties and geometric parameters are given in Table II). We can now employ Eq. 8 to estimate that the required capacitance of the compensation capacitor will be $C_c = 31.0\,\mu$F. As a side note, $C_c = 53.5\,\mu$F is the capacitance required to form an L-C tank resonator with the coil with a resonance that matches the MMRA.

We now experimentally test three important scenarios: (1) using a coil alone as the driving system (i.e., no compensation capacitor), (2) introducing the series compensation capacitor to match the coil resonant with the MMRA resonant frequency (i.e., $C_c = 53.5\,\mu$F), and (3) setting the compensation capacitor to the predicted value (i.e., $C_c = 31.0\,\mu$F). In each scenario, we experimentally measure the FPRW and FPV of the system and compare them to the analytical predictions from Eqs. 3 and 4. As shown in Fig. 4(a), the FPRW of the system in all three scenarios remains unchanged. The slight difference comes from the parasitic resistance intrinsic to the

This work is licensed under a Creative Commons Attribution 4.0 License. For more information, see https://creativecommons.org/licenses/by/4.0/

This article has been accepted for publication in IEEE Transactions on Antennas and Propagation. This is the author's version which has not been fully edited and content may change prior to final publication. Citation information: DOI 10.1109/TAP.2023.3333956

TABLE I
PARAMETERS USED IN EFFICIENCY CALCULATIONS

Parameter	Symbol	Value
Rotor moment of inertia	J	13.7 mm^2g
Damping coefficient	β	39.6 nNm · s/rad
Restoring stiffness	κ	0.1207 Nm/rad
Coupling coefficient	Γ_o	0.64 Nmm/A
Coil inductance	L_c	2.1 mH
Coil resistance	R_c	1.16 Ω
Receiver distance	d	100.14 mm
Angle coefficient	A_θ	0.1443 mT/rad
Current coefficient	A_I	0.1486 mT/A

TABLE II
MATERIAL PROPERTIES AND GEOMETRIC PARAMETERS FOR THE SINGLE-ROTOR MMT

Parameter	Value
Rotor magnet remanence	1.338 T
Rotor length	2.3125 in
Rotor diameter	4 mm
Suspension torsional stiffness	2.2 N mm/rad
Stator magnet remanence	1.355 T
Stator length	3 in
Stator width	0.5 in
Stator height	0.5 in
Center distance between rotor and stator	21.85 mm
Coil inner length	135 mm
Coil inner width	95 mm
Coil outer length	155 mm
Coil outer width	115 mm
Coil thickness	18 mm

ceramic capacitors. The optimal driving frequency for maximizing FPRW is experimentally measured at 472.0 Hz in all scenarios. Fig. 4b presents the simultaneously measured FPV for the three scenarios. We find that the correct compensation capacitance yields an FPV whose resonance is aligned with the FPRW resonance. The FPV on resonance is also 3.2 times higher than that of the system using the coil alone, i.e. without any compensation capacitor and is 1.62 times higher than when the coil and MMRA have the same resonant frequency. The experimental and analytical results confirm that this efficiency optimization method helps maximize the FPV of the system at the optimal driving frequency without affecting the FPRW of the system. From Fig. 4, we can also see that there is a very good agreement between the analytical model (Eqs. 3 and 4) and the experimental data for both the FPRW and FPV.

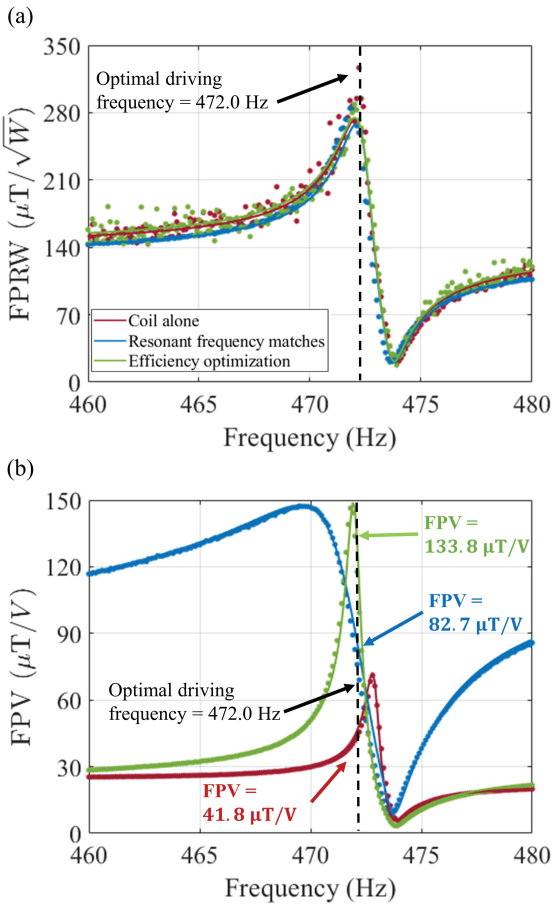

Fig. 4. Analytical (solid lines) and experimental (dots) results of (a) FPRW and (b) FPV of the system at different driving frequencies. Red color represents scenario 1 (no capacitor in the experiment), blue color represents scenario 2 ($C_c = 54.1\,\mu$F in the experiment), and green color represents scenario 3 ($C_c = 29.0\,\mu$F in the experiment). The vertical black dash line marks the optimal driving frequency, which is $\omega_{opt} = 472.0$ Hz in all three scenarios. FPVs of three scenarios at the optimal driving frequency are 41.8 μT/V, 82.7 μT/V, and 133.8 μT/V, respectively, as indicated in (b).

IV. CONCLUSION

In this work, we demonstrate an optimization method that simultaneously maximizes the voltage efficiency and power efficiency of an MMT through the simple addition of a compensation capacitor to the drive coil. Our analytical model exhibits excellent agreement with experimental results. In practical applications, increasing the magnetic moment of an MMT is often necessary to enhance the signal strength or extend the communication distance. One way to achieve this is to use a larger magnet for a single-rotor MMT, while another approach is to employ multiple smaller rotors in a multi-rotor MMT, which offers advantages such as higher power efficiency and higher resonant frequency [5]. In Appendix A, we describe in detail how to leverage this optimization method with multi-rotor MMTs. Importantly, our numerical analysis with multi-rotor MMTs, presented in Appendix B, suggests that the improvement factors can be significantly higher than we have shown in our single-rotor experiments. These findings highlight the potential benefits of this efficiency optimization method and suggest promising directions for future research.

This work is licensed under a Creative Commons Attribution 4.0 License. For more information, see https://creativecommons.org/licenses/by/4.0/

This article has been accepted for publication in IEEE Transactions on Antennas and Propagation. This is the author's version which has not been fully edited and content may change prior to final publication. Citation information: DOI 10.1109/TAP.2023.3333956

APPENDIX A
IMPROVING EFFICIENCY OF MULTI-ROTOR MMTS USING COMPENSATION CAPACITORS

Consider a multi-rotor MMT consisting of a linear chain of rotors and stators driven by a drive coil [5], [6], [14], as shown in Fig. S1. The differential equations that describe an N-rotor MMT system can be written as

$$\begin{cases} L_c\dot{I} + R_cI + \frac{1}{C_c}\int I dt = \mathbf{\Gamma}^{\mathrm{T}}\dot{\mathbf{\Theta}} + V \\ \boldsymbol{J}\ddot{\mathbf{\Theta}} + \boldsymbol{B}\dot{\mathbf{\Theta}} + \boldsymbol{K}\mathbf{\Theta} = -\mathbf{\Gamma}I \end{cases} \tag{A1}$$

where L_c, R_c, and C_c are the inductance, resistance, and capacitance of the coil, respectively. The vector $\mathbf{\Theta} = [\theta_1, \theta_2, ..., \theta_N]^{\mathrm{T}}$ represents the instantaneous angle of each rotor. The vector $\mathbf{\Gamma} = [\Gamma_1, \Gamma_2, ..., \Gamma_N]^{\mathrm{T}}$ represents the coupling where Γ_i is the coupling coefficient between the i^{th} rotor and the drive coil. The inertia matrix $\boldsymbol{J}$ is an $N \times N$ diagonal matrix written as $\boldsymbol{J} = \mathrm{diag}(J_1, J_2, ..., J_N)$ where J_i is the moment of inertia of the i^{th} rotor. The damping matrix $\boldsymbol{B}$ can be expanded into two major contributions $\boldsymbol{B} = \boldsymbol{B}_{sus} + \boldsymbol{B}_{eddy}$. $\boldsymbol{B}_{sus}$ is an $N \times N$ diagonal matrix written as $\boldsymbol{J} = \mathrm{diag}(\beta_1, \beta_2, ..., \beta_N)$ where β_i is the damping coefficient of the i^{th} rotor from its suspension. $\boldsymbol{B}_{eddy}$ is an $N \times N$ matrix that represents the eddy current loss coefficient whose value can be calculated from the model developed in (Ref. [14]). The stiffness matrix $\boldsymbol{K}$ can be expanded into three major contributions $\boldsymbol{K} = \boldsymbol{K}_{sus} + \boldsymbol{K}_r + \boldsymbol{K}_s$. $\boldsymbol{K}_{sus}$ is a diagonal matrix written as $\boldsymbol{K}_{sus} = \mathrm{diag}(\kappa_1, \kappa_2, ..., \kappa_N)$ where κ_i represents the restoring stiffness on the i^{th} rotor from its suspension. $\boldsymbol{K}_r$ and $\boldsymbol{K}_s$ are $N \times N$ matrices that represent the restoring stiffness generated by rotors and stators, respectively, and their values can be calculated from the model developed in (Ref. [14]). The mechanically synchronized mode (i.e., the in-phase mode) is particularly well suited for MMT applications [5], [6] since it has the highest resonant frequency, produces the largest magnetic signal, and couples best to the drive coil (the other modes tend to be magnetically dark) [14]. The oscillation mode shape $\mathbf{\Phi}$ for the in-phase mode of the multi-rotor MMT can be evaluated from the eigenvector of the matrix $\boldsymbol{J}^{-1}\boldsymbol{K}$. The differential equations can be rewritten as

$$\begin{cases} L_c\dot{I} + R_cI + \frac{1}{C_c}\int I dt = \mathbf{\Gamma}^{\mathrm{T}}\mathbf{\Phi}\dot{\theta}_e + V \\ \mathbf{\Phi}^{\mathrm{T}}\boldsymbol{J}\mathbf{\Phi}\,\ddot{\theta}_e + \mathbf{\Phi}^{\mathrm{T}}\boldsymbol{B}\mathbf{\Phi}\,\dot{\theta}_e + \mathbf{\Phi}^{\mathrm{T}}\boldsymbol{K}\mathbf{\Phi}\,\theta_e = -\mathbf{\Phi}^{\mathrm{T}}\mathbf{\Gamma}I \end{cases} \tag{A2}$$

where θ_e is the effective oscillation angle such that $\mathbf{\Theta} = \mathbf{\Phi}\theta_e$. We can further simplify Eq. A2 into this form:

$$\begin{cases} L_c\dot{I} + R_cI + \frac{1}{C_c}\int I dt = \Gamma_e\dot{\theta}_e + V \\ J_e\ddot{\theta}_e + \beta_e\dot{\theta}_e + \kappa_e\theta_e = -\Gamma_e I \end{cases} \tag{A3}$$

where $\Gamma_e = \mathbf{\Gamma}^{\mathrm{T}}\mathbf{\Phi} = \mathbf{\Phi}^{\mathrm{T}}\mathbf{\Gamma}$ is the effective coupling coefficient, $J_e = \mathbf{\Phi}^{\mathrm{T}}\boldsymbol{J}\mathbf{\Phi}$ is the effective moment of inertia, $\beta_e = \mathbf{\Phi}^{\mathrm{T}}\boldsymbol{B}\mathbf{\Phi}$ is the effective damping coefficient, and $\kappa_e = \mathbf{\Phi}^{\mathrm{T}}\boldsymbol{K}\mathbf{\Phi}$ is the effective stiffness of the multi-rotor MMT. The magnetic field at the receiver along the $\hat{x}$ direction can be written as

$$B_{total}(t) = A_{\theta_e}\theta_e(t) + A_I I(t)\ . \tag{A4}$$

where A_I is the current coefficient and A_{θ_e} is the effective angle coefficient. Under the dipole approximation and the small angle approximation, the effective angle coefficient can be evaluated as

$$A_{\theta_e} = \boldsymbol{A_\theta}\mathbf{\Phi} \tag{A5}$$

where $\boldsymbol{A_\theta} = -[\frac{\mu_0 M_{r,1}}{2\pi d^3}, \frac{\mu_0 M_{r,2}}{2\pi d^3}, ..., \frac{\mu_0 M_{r,N}}{2\pi d^3}]$. Therefore, using Eqs. A3 and A4, we can follow the same procedure and apply the efficiency optimization method described in the main manuscript on multi-rotor MMTs.

APPENDIX B
NUMERICAL ANALYSIS FOR MULTI-ROTOR MMTS

Let us consider a multi-rotor MMT with N identical rotors and suspension systems, and the same resonant frequency ω_{res} as the single-rotor MMT, i.e., assuming i as the rotor index we have $J_i = J_r$, $\beta_i = \beta_r$, and $\kappa_i = \kappa_r$ for all individual rotors. As a reminder, ω_{res} is the resonance for the transfer function $H_{\theta/I}(\omega)$, and it is only set by the mechanics in our model. For simplicity we can also assume the N-rotor MMT has an uniform mode shape, i.e., $\mathbf{\Phi}$ is an identity matrix, and thus $J_e = NJ_r$, $\beta_e = N\beta_r$, and $\kappa_e = N\kappa_r$. Here it is important to emphasize that in a real multi-rotor system the rotor participation is generally non-uniform, and the synchronized oscillation mode of a multi-rotor MMT typically has a much higher frequency ω_{res} than the individual rotors [14]. For the sake of simplicity and insight development, we will choose to ignore these subtleties, but details for interested readers can be found in [14].

Based on the above assumptions, we find that as the number of rotors N increases, the coil size will need to increase to accommodate the size of the rotor array. Since both coil size (and thus the coil inductance and resistance) and magnetic moment increase by a factor of N, the coupling coefficient increases by a factor of N^2 as it linearly depends on both the coil size and the magnetic moment [5], i.e., $\Gamma_e = N^2\Gamma_r$. If we assume this rapid scaling on the coupling coefficient and maintain the above assumptions on individual rotors, it can be shown that there will be a more substantial improvement in the FPV of the MMT when a compensation capacitor is used. Since the analytical arguments for this conclusion are not easily presented, we instead conducted numerical simulations for MMTs with varying numbers of rotors $N = 1, 5, 10, 20$. The results of this numerical analysis are presented in Fig. B1. This analysis confirms that, for larger numbers of rotors, the improvement in FPV can be significantly higher than what we have reported in single-rotor MMT experiments conducted in the main manuscript. These findings highlight the potential benefits of this efficiency optimization method for multi-rotor systems.

ACKNOWLEDGMENT

This work was sponsored by the Defense Advanced Research Projects Agency (DARPA) grant HR0011-17-2-0057 under the A MEchanically Based Antenna (AMEBA) program.

This work is licensed under a Creative Commons Attribution 4.0 License. For more information, see https://creativecommons.org/licenses/by/4.0/

This article has been accepted for publication in IEEE Transactions on Antennas and Propagation. This is the author's version which has not been fully edited and content may change prior to final publication. Citation information: DOI 10.1109/TAP.2023.3333956

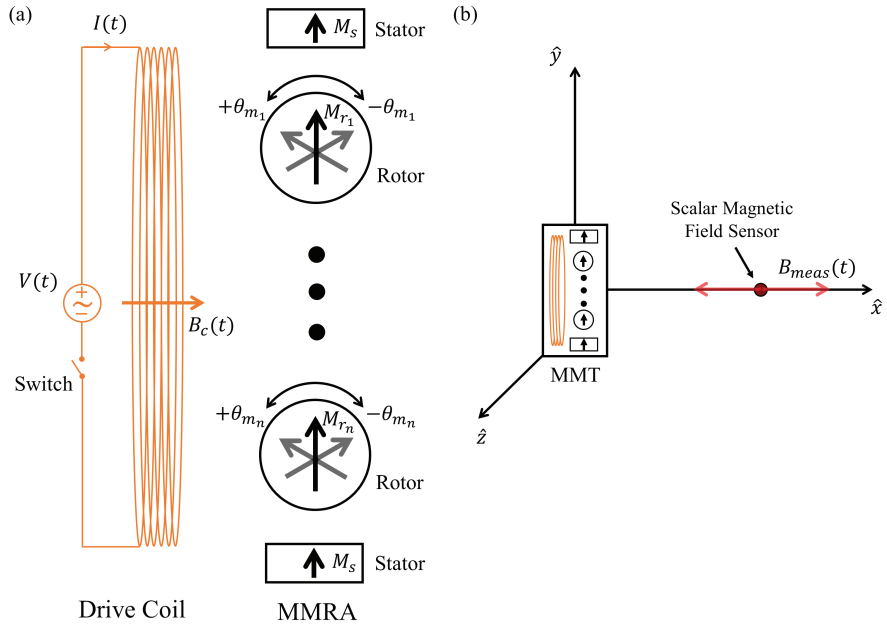

Fig. A1. The operational principle of a multi-rotor MMT. (a) Schematic diagram of a multi-rotor MMT. The rotors and stators in the MMT have uniform magnetization, $\vec{M}_{r_i}$ and $\vec{M}_s$, respectively, pointing in the $\hat{y}$ direction at rest, which is orthogonal to $\vec{B}_c(t)$ to maximize the drive torque on the rotor. (b) Schematic diagram showing the relative position of the MMT and the receiver (scalar magnetic field sensor).

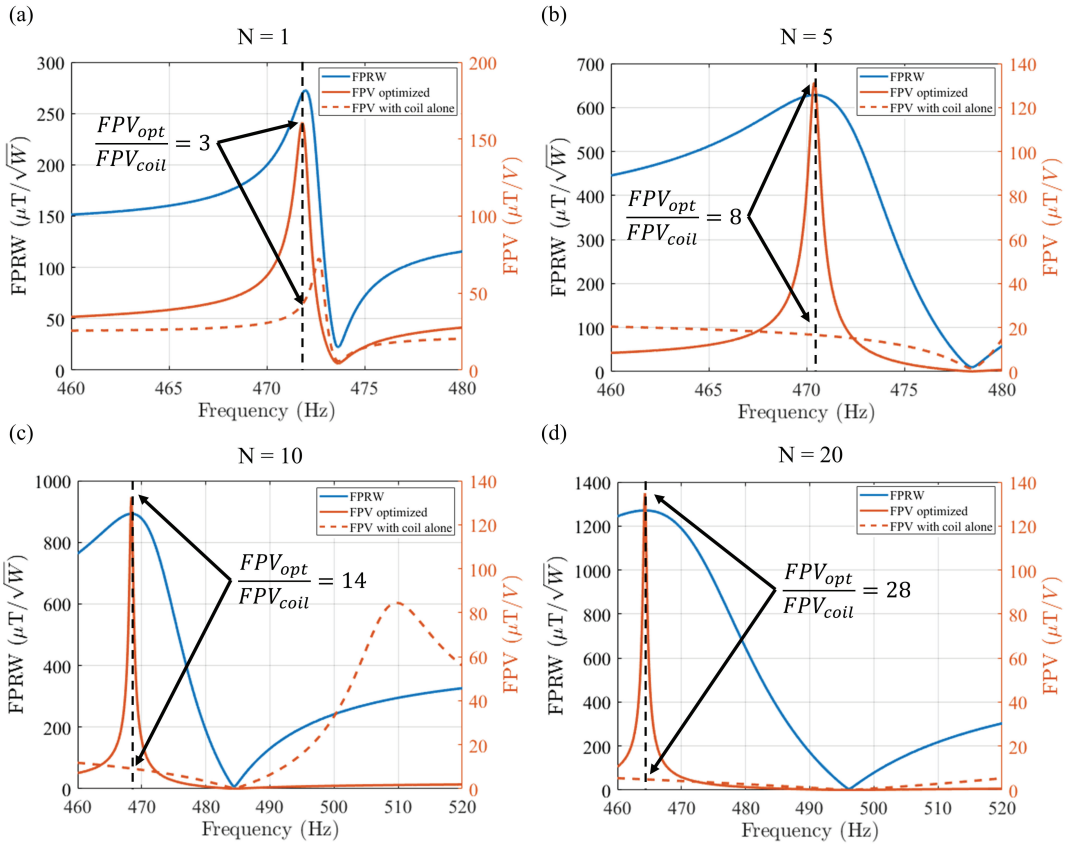

Fig. B1. Numerical results for MMTs with varying numbers of rotors (N = 1, 5, 10, and 20) at different driving frequencies. The solid blue lines represent the simulated FPRW of the MMTs. The dashed orange lines present the simulated FPV of the system with the coil alone (FPV_{coil}, scenario 1 from the main manuscript). In contrast, the solid orange lines present the simulated FPV of the system with the capacitor-based efficiency optimization applied for each individual case (FPV_{opt}, scenario 3 from the main manuscript). The vertical black dashed lines indicate the optimal driving frequencies and the improvement factors (measured as FPV_{opt}/FPV_{coil}) are indicated in the plots. The results show that significantly higher factors of improvement are possible than in the single-rotor MMT case.

This work is licensed under a Creative Commons Attribution 4.0 License. For more information, see https://creativecommons.org/licenses/by/4.0/

This article has been accepted for publication in IEEE Transactions on Antennas and Propagation. This is the author's version which has not been fully edited and content may change prior to final publication. Citation information: DOI 10.1109/TAP.2023.3333956

REFERENCES

[1] D. M. Pozar, *Microwave Engineering*. Chichester, England: John Wiley & Sons, 4 ed., Nov. 2011.

[2] A. Watt, *VLF Radio Engineering*. International series of monographs on electromagnetic waves, Pergamon Press, 1967.

[3] A. Gigliotti, W. Gekelman, P. Pribyl, S. Vincena, A. Karavaev, X. Shao, A. S. Sharma, and D. Papadopoulos, "Generation of polarized shear alfvén waves by a rotating magnetic field source," *Physics of Plasmas*, vol. 16, p. 092106, Sept. 2009.

[4] J. R. Wait, "Project sanguine," *Science*, vol. 178, pp. 272–275, Oct. 1972.

[5] R. P. Thanalakshme, A. Kanj, J. Kim, E. Wilken-Resman, J. Jing, I. H. Grinberg, J. T. Bernhard, S. Tawfick, and G. Bahl, "Magneto-mechanical transmitters for ultralow frequency near-field data transfer," *IEEE Transactions on Antennas and Propagation*, vol. 70, no. 5, pp. 3710–3722, 2022.

[6] M. N. Srinivas Prasad, R. U. Tok, F. Fereidoony, Y. E. Wang, R. Zhu, A. Propst, and S. Bland, "Magnetic pendulum arrays for efficient ULF transmission," *Scientific Reports*, vol. 9, Sept. 2019.

[7] S. Gong, Y. Liu, and Y. Liu, "A rotating-magnet based mechanical antenna (RMBMA) for ELF-ULF wireless communication," *Progress In Electromagnetics Research M*, vol. 72, pp. 125–133, 2018.

[8] M. N. S. Prasad, S. Selvin, R. U. Tok, Y. Huang, and Y. Wang, "Directly modulated spinning magnet arrays for ULF communications," in *2018 IEEE Radio and Wireless Symposium (RWS)*, pp. 171–173, 2018.

[9] H. Rezaei, V. Khilkevich, S. Yong, D. S. Stutts, and D. Pommerenke, "Mechanical magnetic field generator for communication in the ULF range," *IEEE Transactions on Antennas and Propagation*, vol. 68, no. 3, pp. 2332–2339, 2020.

[10] H. C. Burch, A. Garraud, M. F. Mitchell, R. C. Moore, and D. P. Arnold, "Experimental generation of ELF radio signals using a rotating magnet," *IEEE Transactions on Antennas and Propagation*, vol. 66, no. 11, pp. 6265–6272, 2018.

[11] J. S. Glickstein, J. Liang, S. Choi, A. Madanayake, and S. Mandal, "Power-efficient ELF wireless communications using electro-mechanical transmitters," *IEEE Access*, vol. 8, pp. 2455–2471, 2020.

[12] S. Yang, J. Xu, M. Guo, B. Zhang, C. Lan, H. Li, and K. Bi, "Progress on very/ultra low frequency mechanical antennas," *ES Materials & Manufacturing*, vol. 16, pp. 1–12, 2022.

[13] A. Kanj, R. P. Thanalakshme, C. Li, J. Kulikowski, G. Bahl, and S. Tawfick, "Design, dynamics, and dissipation of a torsional-magnetic spring mechanism," *Mechanical Systems and Signal Processing*, vol. 179, p. 109307, Nov. 2022.

[14] J. Jing, S. Tawfick, and G. Bahl, "Frequency response and eddy current power loss in magneto-mechanical transmitters," *IEEE Transactions on Antennas and Propagation*, vol. 71, no. 4, pp. 3642–3653, 2023.

[15] J. D. Jackson and L. C. Levitt, "Classical electrodynamics," *Physics Today*, vol. 15, pp. 62–62, Nov. 1962.

[16] D. Hamill, "Lumped equivalent circuits of magnetic components: the gyrator-capacitor approach," *IEEE Transactions on Power Electronics*, vol. 8, pp. 97–103, Apr. 1993.

Jiheng Jing received a B.S. degree in mechanical engineering from the University of Illinois at Urbana-Champaign, Champaign, IL, USA, in 2019. He is currently pursuing a Ph.D. degree in mechanical engineering at the University of Illinois. His research interests include magneto-mechanical systems, linear and nonlinear dynamic analysis, eddy current analysis, and optimized mechanical suspension design.

Gaurav Bahl (M'10, SM'16) received the B.Eng. degree in Electrical Engineering from McMaster University, Hamilton, ON, Canada, in 2005, and M.S. and Ph.D. degrees in Electrical Engineering from Stanford University, Stanford, CA, in 2008 and 2010 respectively. His graduate work at Stanford University focused on studying dielectric charging in microelectromechanical systems and drift stability of encapsulated silicon microresonators. He pursued his postdoctoral work from 2010-2012 at the University of Michigan, Ann Arbor, developing optomechanical oscillators for frequency reference applications.

He is currently the George B. Grim Professor of Mechanical Science and Engineering at the University of Illinois at Urbana-Champaign, is an Affiliate in the ECE and Physics Departments, and with the Illinois Quantum Information Science and Technology Center (IQUIST). His research interests include integrated photonics and nonlinear optics, especially Brillouin optomechanics, nonreciprocal systems, topological metamaterials, and optomechanofluidic devices. He is a recipient of the Presidential Early Career Award for Scientists and Engineers (PECASE) in 2019, the UIUC Dean's Award for Excellence in Research, the ONR Director of Research Early Career Grant in 2016, and the AFOSR Young Investigator Award in 2015. He is currently Senior Member of IEEE since 2016 and a Fellow of Optica (formerly OSA) since 2022.

This work is licensed under a Creative Commons Attribution 4.0 License. For more information, see https://creativecommons.org/licenses/by/4.0/